SCIENTIFIC REPORTS

OPEN

Mitigation of severe urban haze pollution by a precision air pollution control approach

Shaocai Yu[1,2], Pengfei Li[1], Liqiang Wang[1], Yujie Wu[1], Si Wang[1], Kai Liu[2], Tong Zhu[3], Yuanhang Zhang[3], Min Hu[3], Liming Zeng[3], Xiaoye Zhang[4], Junji Cao[5], Kiran Alapaty[6], David C. Wong[7], Jon Pleim[7], Rohit Mathur[7], Daniel Rosenfeld[8] & John H. Seinfeld[2]

Severe and persistent haze pollution involving fine particulate matter ($PM_{2.5}$) concentrations reaching unprecedentedly high levels across many cities in China poses a serious threat to human health. Although mandatory temporary cessation of most urban and surrounding emission sources is an effective, but costly, short-term measure to abate air pollution, development of long-term crisis response measures remains a challenge, especially for curbing severe urban haze events on a regular basis. Here we introduce and evaluate a novel precision air pollution control approach (PAPCA) to mitigate severe urban haze events. The approach involves combining predictions of high $PM_{2.5}$ concentrations, with a hybrid trajectory-receptor model and a comprehensive 3-D atmospheric model, to pinpoint the origins of emissions leading to such events and to optimize emission controls. Results of the PAPCA application to five severe haze episodes in major urban areas in China suggest that this strategy has the potential to significantly mitigate severe urban haze by decreasing $PM_{2.5}$ peak concentrations by more than 60% from above 300 μg m^{-3} to below 100 μg m^{-3}, while requiring ~30% to 70% less emission controls as compared to complete emission reductions. The PAPCA strategy has the potential to tackle effectively severe urban haze pollution events with economic efficiency.

China's unprecedented urbanization has been accompanied by an increase in the level of air pollution (both indoor and outdoor), which has been estimated to lead to 2.5 million premature deaths annually[1–4]. To tackle the increased threat owing to the growth of regional air pollution, in 2010 the State Council of China issued the circular, "Regional Joint Prevention and Control of Air Pollution", to enhance the effort in regional environmental protection and reduction of the overall emissions of air pollutants[5]. The increased frequency of long-duration "haze episodes" with record-breaking air pollutant concentrations has become the most conspicuous feature of air pollution in China[6–9]. A "Haze day" is defined as one with visibility <10 km under conditions of 80% relative humidity and mainly caused by elevated $PM_{2.5}$ (particles with aerodynamic diameter <2.5 μm) concentrations[10–12]. Such severe haze episodes occur predominantly in the economically developed, highly industrialized, and densely populated areas in China, such as the three largest urban regions (i.e., Beijing-Tianjin-Hebei (BTH), Yangtze River Delta (YRD) and Pearl River Delta (PRD)) and six urban mega-cities (i.e., central Liaoning, Shandong Peninsula, Wuhan and its surrounding areas, Chang-Zhu-Tan, Chengdu-Chongqing and Taiwan Strait West Coast)[6–9,13–16]. In January 2013, for example, unprecedented severe haze episodes with peak hourly $PM_{2.5}$

[1]Research Center for Air Pollution and Health; Key Laboratory of Environmental Remediation and Ecological Health, Ministry of Education, College of Environmental and Resource Sciences, Zhejiang University, Hangzhou, Zhejiang, 310058, P.R. China. [2]Division of Chemistry and Chemical Engineering, California Institute of Technology, Pasadena, CA, 91125, USA. [3]College of Environmental Sciences and Engineering, Peking University, Beijing, 100871, P.R. China. [4]Key Laboratory for Atmospheric Chemistry, Chinese Academy of Meteorological Sciences, CMA, 46 Zhong Guan Cun S. Ave., Beijing, 100081, China. [5]Key Lab of Aerosol Chemistry and Physics, SKLLQG, Institute of Earth Environment, Chinese Academy of Sciences, Xi'an, China. [6]Systems Exposure Division, National Exposure Research Laboratory, U.S. Environmental Protection Agency (EPA), Research Triangle Park, NC, 27711, USA. [7]Computational Exposure Division, National Exposure Research Laboratory, U.S. Environmental Protection Agency (EPA), Research Triangle Park, NC, 27711, USA. [8]Institute of Earth Sciences, The Hebrew University of Jerusalem, Jerusalem, Israel. Shaocai Yu, Pengfei Li and Liqiang Wang contributed equally to this work. Correspondence and requests for materials should be addressed to S.Y. (email: shaocaiyu@zju.edu.cn) or K.A. (email: Alapaty.Kiran@epa.gov) or J.H.S. (email: Seinfeld@caltech.edu).

concentrations of ~1000 μg m^{-3} occurred in central eastern China[6,7] enveloping over 10^6 km². To address severe haze pollution in China, the "Action Plan on Prevention and Control of Air Pollution" (referred to as the "Country Ten" measures), the nation's most stringent measures to control haze historically, was released by China's State Council in 2013[17]. The Action Plan aimed, for example, to reduce PM$_{2.5}$ in the Beijing-Tianjin-Hebei region by 25% by 2017 relative to 2012 levels.

Studies of the sources and formation mechanisms of severe PM$_{2.5}$ episodes in China pinpoint emissions from coal-combustion, motor vehicle traffic, construction dust, cooking, and agricultural activities (such as biomass burning), in conjunction with concomitant stagnant meteorological conditions (a shallow atmospheric boundary layer, temperature inversion, low wind speed, and high relative humidity)[6,7,13–15]. In addition to massive amounts of primary emissions, secondary PM products from the oxidation of precursors, such as SO$_2$, NO$_x$, and volatile organic compounds (VOCs), are estimated to make a significant contribution (30–70%) to PM$_{2.5}$ during these severe haze pollution events[6,7,13–15]. Regional transport of emissions from upwind areas also contributes significantly to haze pollution in the urban areas[13,15]. Despite intensive measures, such as coal combustion reduction, traffic and dust emission controls, significant improvements have not resulted, especially for severe winter haze episodes, as reported by the Xinhua news agency and China's Ministry of Environmental Protection (MEP)[18–22]. In 2016, for example, 80% of Chinese cities failed to meet air quality standards, and red alerts were triggered (China has a four-tier, color-coded warning system, with red being the most serious, followed by orange, yellow and blue) in more than 20 cities in early January, 2017[21]. The mean PM$_{2.5}$ concentration in 338 Chinese cities in January, 2017, was 78 μg m^{-3}, 14.7% higher than in the previous year, especially in the Beijing-Tianjin-Hebei area, where the mean PM$_{2.5}$ concentration was 128 μg m^{-3}, 43.8% higher than in 2016[22].

By contrast, good air quality was achieved for several large international events, such as the 2008 Beijing Olympics, 2010 Shanghai Expo, 2014 Beijing Asia-Pacific Economic Cooperation (APEC) Summit, 2015 Beijing Grand Military Parade, and the 2016 G20 Hangzhou Summit, as a result of stringent urban and regional emission control measures enacted in anticipation of these events[23–27]. These measures involved mandatory temporary closure of most industrial emission sources in the host city and its surrounding areas. For example, it was estimated that the short-term crisis response measures for the 2014 APEC summit resulted in average reduction rates of 39.2, 49.6, 66.6, 61.6, and 33.6% for the emissions of SO$_2$, NO$_x$, PM$_{10}$, PM$_{2.5}$ and volatile organic compounds (VOCs) in Beijing, respectively[28]. Despite these particular successes, establishing a long-term air pollution control strategy for curbing severe urban haze on a regular basis poses a continuing challenge.

A red alert for severe haze pollution was issued for Beijing on December 8, 2015, extending from 7 am on December 8 until 12:00 am on December 10 (local time) in order to "protect public health and reduce levels of severe air pollution" as stated in Beijing Municipal Environmental Protection Bureau's official Weibo account[29]. Such a "red alert" is released when severe air pollution with the air quality index (AQI) >500 is forecasted to persist longer than 3 days (72 h). Mandatory and recommended emergency response plans include[30]: (1) Suspending 50% motor vehicle traffic and extending operating hours of public transportation; (2) Barring heavy-duty vehicles from the roads; (3) Banning all construction activities; (4) Washing roads at least once daily to reduce traffic dust; and (5) Banning fireworks and outdoor barbecues. Additional recommended emergency measures include: (1) Schools closed and enterprises encouraged to adopt flexible working schedules and (2) Large-scale outdoor activities banned[30]. Both mandatory and recommended emergency responses triggered by the first-ever smog red alert issued by the Beijing government on December 7, 2015, led only to 10% lower PM$_{2.5}$ concentrations, with the PM$_{2.5}$ concentration in Beijing reaching 233 μg m^{-3} at 5 pm on December 9, despite suspension of production at about 2,100 companies and of outdoor work at ~3,500 construction sites[31]. This was likely a result of the fact that the actual sources contributing to the severe haze during this episode had not been targeted effectively.

Large-scale comprehensive atmospheric chemical transport models are used extensively to evaluate the effectiveness of emission control strategies in a retrospective manner[32]. Source apportionment methods, mainly including emission inventories, 3-D air quality models and receptor models, are used to identify and quantify the major sources of PM and to provide the scientific basis for emission control measures with different short-comings and uncertainties for each method[32–35]. In this work, we propose a new air pollution control strategy, to be implemented when impending meteorological conditions portend a pollution episode. Using a hybrid trajectory-receptor model in conjunction with a state-of-the-art 3-D atmospheric chemical transport model and high PM$_{2.5}$ concentrations, either observed or forecast, those emission areas that are predicted to most heavily influence air quality levels in the major urban area are identified. We term this a Precision Air Pollution Control Approach (PAPCA), in that the strategy takes advantage of the predictive power of comprehensive atmospheric chemical transport models, offering effectiveness, practicality, and economic efficiency for significantly mitigating impending severe urban haze pollution. To the best of our knowledge, this paper is first to combine all three components (high PM$_{2.5}$ concentrations (either observed or forecast), a hybrid trajectory-receptor model and a comprehensive 3-D air quality model) together to pinpoint the origins of emissions leading to heavy haze events and to optimize emission controls.

Results and Discussion

The essential idea of the PAPCA is to predict the advent of extreme pollutant concentrations using a comprehensive 3-D air quality model in conjunction with a hybrid trajectory-receptor model to calculate so-called Concentration Weighted Trajectory (CWT) values which can pinpoint the emission areas that are predicted to contribute most significantly to a pending severe urban haze event. The comprehensive 3-D air quality model is employed to optimize the emission controls that will most effectively mitigate the impending haze event. The CWT values are used as a weighting function for emission control factors when the emission control schemes for the targeted areas are optimized in the 3-D atmospheric chemical transport model simulations. In short, the targeted emission areas with the highest potential contributions to the severe haze episode are identified by the CWT values (See Methods).
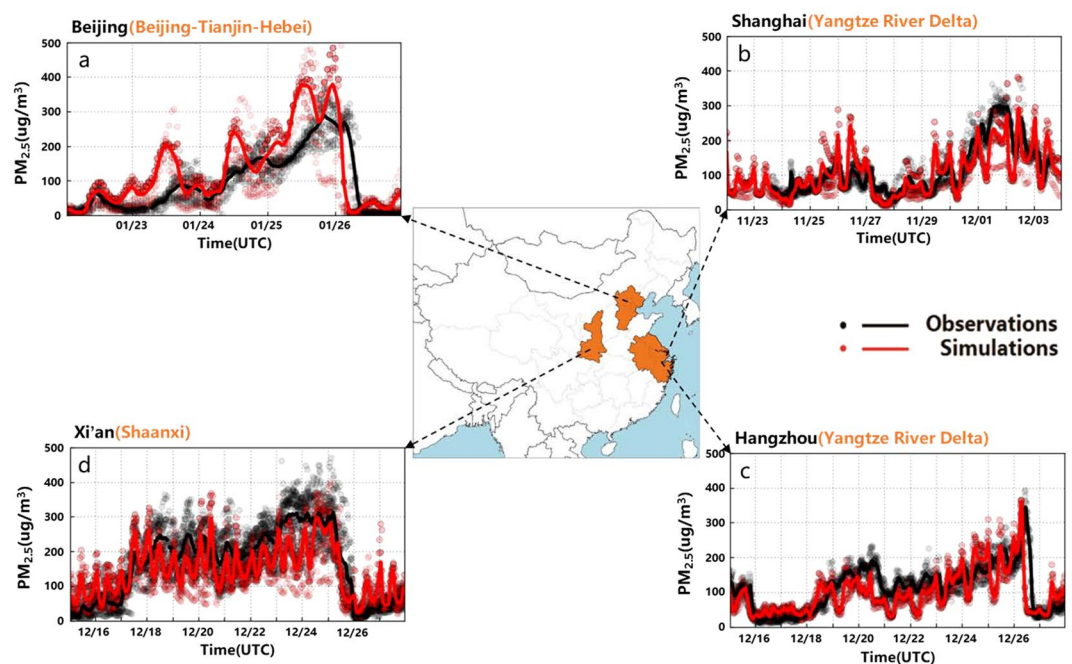
Figure 1. 12-km grid resolution model domain (central panel) and time-series comparisons of WRF-CMAQ model predictions and observations for hourly $PM_{2.5}$ concentrations. (**a**) Time-series comparison of predicted and observed hourly $PM_{2.5}$ concentrations at 12 monitoring stations in Beijing from Jan 22 to 26, 2017. (**b**) The same as (**a**) but at 10 monitoring stations in Shanghai for the period from Nov 24 to Dec 4, 2013. (**c**) The same as (**a**) but at 10 monitoring stations in Hangzhou for the period from December 15 to Dec 28, 2013. (**d**) The same as (**a**) but at 13 monitoring stations in Xi'an for the period from December 15 to Dec 28, 2013. The solid lines represent hourly mean concentrations in each city and each dot represents the hourly observation at each surface monitoring station in each city as listed in Table S1.

To illustrate how the application of the PAPCA might have worked, we focus on four severe urban haze outbreaks in 2013 in Beijing, Shanghai, Hangzhou, and Xian, which are located in the northern, eastern, eastern and western regions of China, respectively, and one severe urban haze episode in 2017 in Beijing (Figs 1 and S1). Observed hourly peak $PM_{2.5}$ concentrations were 376, 376, 394, and 941 $\mu g\,m^{-3}$ for the 2013 outbreaks in Beijing, Shanghai, Hangzhou, and Xian, respectively, each substantially exceeding the daily national $PM_{2.5}$ air quality standard of 75 $\mu g\,m^{-3}$. Observed $PM_{2.5}$ concentrations in Beijing rapidly increased from 67 $\mu g\,m^{-3}$ at 18:00 on October 26 to 376 $\mu g\,m^{-3}$ at 23:00 on October 28 and then sharply decreased to about 20 $\mu g\,m^{-3}$ by 3:00 on October 29 (Fig. S1a). $PM_{2.5}$ concentrations rose in a second cycle from 107 $\mu g\,m^{-3}$ at 15:00 on October 30 to 355 $\mu g\,m^{-3}$ at 15:00 on November 2, then sharply decreasing from ~256 $\mu g\,m^{-3}$ at 2:00 to 43 $\mu g\,m^{-3}$ at 3:00 on November 3 within a one-hour time frame (Fig. 1a). The 48-h air mass back trajectories (Fig. S2b) show that the severe haze periods in Beijing were influenced mainly by air masses from the southwest and east of Beijing, especially the southwest areas. The eventual sharp decrease of $PM_{2.5}$ in Beijing was associated with a change in air mass wind direction from southwesterly to northwesterly, bringing clean air masses from Inner Mongolia and Mongolia areas to Beijing[30]. Similarly, the haze period in Beijing in 2017 with $PM_{2.5}$ >150 $\mu g\,m^{-3}$ was influenced mainly by air masses from the southwest of Beijing (Fig. 1a), and $PM_{2.5}$ concentrations sharply decreased from ~299 $\mu g\,m^{-3}$ at 4:00 am on January 26 to ~13 $\mu g\,m^{-3}$ at 9:00 am on January 26, 2017, because of a change in air mass wind direction from southwesterly to northwesterly (Figs 1a, 2b and S2a). The severe haze period in Shanghai, lasting from 11:00 on November 30 to 5:00 on December 3 with $PM_{2.5}$ >150 $\mu g\,m^{-3}$, was influenced mainly by air masses originating from Zhejiang, Anhui, Jiangsu, Shandong, and Hebei provinces over high emission industrial areas at low wind speed (Figs 1b and S3f)[36]. Similarly, the haze period in Hangzhou with $PM_{2.5}$ >150 $\mu g\,m^{-3}$ was influenced predominantly by air masses originating from the northern industrial part of Hangzhou (Anhui, Jiangsu, Shandong, and Hebei provinces) (Figs 1c and S4f)[37]. In contrast to these three cases, the severe haze period in Xian with $PM_{2.5}$ >150 $\mu g\,m^{-3}$, by application of this method, is found to be influenced by air masses essentially from all directions (Figs 1d and S5f).

In demonstrating the PAPCA, the two-way coupled WRF-CMAQ model (see Methods and SI) was used to simulate each of these four 2013 severe urban haze episodes in retrospective mode and the 2017 severe urban haze episode in forecast mode. The performance of the WRF-CMAQ model simulations of $PM_{2.5}$, O_3, SO_2, NO_2 and CO for these episodes was evaluated extensively by comparison with observations in each city and related surroundings (see Figs 1 and SI). The model performances for $PM_{2.5}$ chemical composition on the basis of available measurements for the Beijing, Shanghai, Hangzhou and Xian cases in the retrospective simulations are summarized in Tables S6a, S6b, S6c and S6d, respectively, and the temporal variations of comparisons of predictions and observations for each $PM_{2.5}$ component are shown in Figs S15–S18. The model captures with reasonable
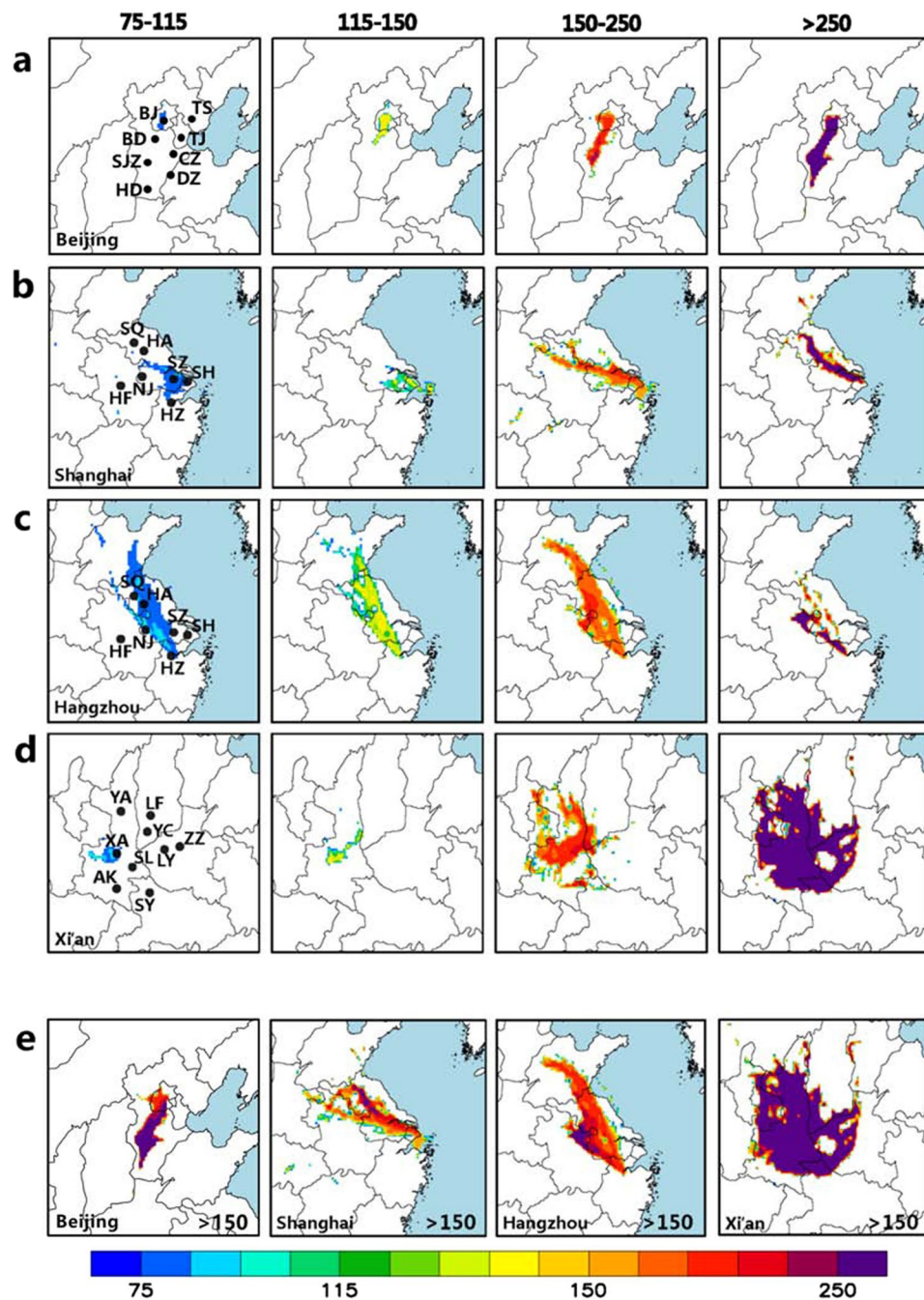
Figure 2. CWT values for $PM_{2.5}$ obtained from the hybrid receptor model to pinpoint origins of heavy haze pollution. (**a**) The spatial distributions of the four different CWT value intervals ($75\,\mu g\,m^{-3} \leq CWT \leq 115\,\mu g\,m^{-3}$, $115\,\mu g\,m^{-3} \leq CWT \leq 150\,\mu g\,m^{-3}$, $150\,\mu g\,m^{-3} \leq CWT \leq 250\,\mu g\,m^{-3}$, $CWT \geq 250\,\mu g\,m^{-3}$) for $PM_{2.5}$ in Beijing for the period from Jan 24 to 26, 2017. (**b**) The same as (**a**) but for the period from Nov 24 to Dec 4, 2013, in Shanghai. (**c**) The same as (**a**) but for the period from December 15 to Dec 28, 2013, in Hangzhou. (**d**) The same as (**a**) but for the period from December 15 to Dec 28, 2013, in Xian. (**e**) The spatial distributions of the CWT values in the four cities for the cases with $CWT \geq 150\,\mu g\,m^{-3}$, AK: Ankang, BD: Baoding, BJ: Beijing, CZ: Cangzhou, DZ: Dezhou, HA: Huai'an, HD: Handan, HF: Hefei, HZ: Hangzhou, LF: Linfen, LY: Luoyang, NJ: Nanjing, SH: Shanghai, SJZ: Shijiazhuang, SL: Shangluo, SQ: Suqian, SY: Shiyan, SZ: Suzhou, TJ: Tianjin, TS: Tangshan, XA: Xi'an, YA: Yan'an, YC: Yuncheng, ZZ: Zhengzhou.

fidelity the hourly variations and broad synoptic changes in the observed $PM_{2.5}$ concentrations for each of the four cities (Fig. 1, Figs S6–S14, and Tables S2–S5). The model exhibits reasonable performance for $PM_{2.5}$ chemical composition for different heavy haze episodes in different cases (see SI). The normalized mean bias (NMB) values for predictions of $PM_{2.5}$ at Beijing, Shanghai, Hangzhou and Xian are −2.8%, −14.5%, −11.4%% and −11.1%, respectively (Tables S2–S5). The results demonstrate skill in reproducing the urban $PM_{2.5}$, O_3, SO_2, NO_2 and CO concentrations, and $PM_{2.5}$ chemical composition for these haze episodes.

A critical aspect of the development of PAPCA strategies is identification of influential sources and their locations leading to specific severe urban haze episodes. Here, 48-h back trajectories and trajectory cluster analyses are used to locate regional transport pathways and relative contributions of air masses influencing the receptor sites for different periods on the basis of observed $PM_{2.5}$ concentration intervals (see Figs S2–S5 and SI). As expected, the severe urban haze episodes were caused by air masses passing over heavily industrialized areas before arriving at the receptor sites. For example, most of the back trajectories with $PM_{2.5} \geq 150 \mu g\, m^{-3}$ in Beijing (mainly belonging to E-SW and SW clusters) were influenced by the heavily industrialized area southwest of Beijing (Figs S1b(f), S1b(g), S2b(f) and S2b(g)). In Shanghai, the severe haze periods with $PM_{2.5} \geq 150 \mu g\, m^{-3}$ were principally affected by air masses (mainly belonging to NW-S and NW-W clusters) from the industrialized northwest of Shanghai (Figs S3f and S3g). In Hangzhou, upwind air masses came from the industrialized northwest and north of Hangzhou (Fig. S4). As noted above, the severe haze periods in Xian were the results of air masses from all directions (Fig. S5).

To pinpoint the source locations with the largest potential contributions to high concentration values at the receptor site, concentration weighted trajectory (CWT) values for $PM_{2.5}$ are calculated on the basis of the air mass back trajectories and their associated $PM_{2.5}$ concentrations (see Methods). We separated the entire dataset into four different categories on the basis of observed $PM_{2.5}$ concentrations: $75 \mu g\, m^{-3} \leq PM_{2.5} < 115 \mu g\, m^{-3}$, $115 \mu g\, m^{-3} \leq PM_{2.5} < 150 \mu g\, m^{-3}$, $150 \mu g\, m^{-3} \leq PM_{2.5} < 250 \mu g\, m^{-3}$, $PM_{2.5} \geq 250 \mu g\, m^{-3}$ and $PM_{2.5} \geq 150 \mu g\, m^{-3}$ when the back trajectories (see Figs S2–S5 and SI) and the CWT values are calculated (see Figs 2 and S1b). The spatial distributions of the four CWT intervals for the five urban cases in Figs 2 and S1b reveal the relative contributions of the potential sources to the high $PM_{2.5}$ concentrations at each of the receptor cities. For example, the main sources affecting the severe haze formation in Beijing with $CWT \geq 250 \mu g\, m^{-3}$ are located in Dezhou, Changzhou, Baoding, Shijiazhuan, Handan, and Tangshang (Fig. S1b), while in Shanghai, they are located in Suzhou, Suqian, Huaian and Bengbu and Nanjing (Fig. 2b). The principal sources affecting Hangzhou with $CWT \geq 150 \mu g\, m^{-3}$ are located in the central part of Jiangsu province (such as Suzhou, Suqian, Huaian, Lianyungang, Bengbu and Nanjing), central part of Shangdong province (such as Rizhao and Jinan) and northern part of Anhui province (Fig. 2c). A close inspection of Figs 2a and S1b for two Beijing cases (one in 2013 and another in 2017) indicates that the main sources affecting the severe haze formation in Beijing with $CWT \geq 250 \mu g\, m^{-3}$ for both cases are located in southwest of Beijing with slightly broader source regions for the 2013 episode. In contrast to the three other cities, the sources affecting haze formation in Xian with $CWT \geq 250 \mu g\, m^{-3}$ are predicted to have originated from all surrounding industrial cities (Fig. 2d). $PM_{2.5}$ concentrations for the haze episode in Xian were consistently $>200 \mu g\, m^{-3}$ with the hourly peak $PM_{2.5}$ concentration of $941 \mu g\, m^{-3}$, substantially exceeding the levels in the other three episodes (Fig. 1).

To evaluate the effectiveness of the PAPCA strategy, emission control factors (ECFs) for the domain were calculated on the basis of the CWT values as follows:

$$
ECFs = \begin{cases} 0.0 \text{ if } CWT \leq 75\ \mu g\ m^{-3} \\ \dfrac{CWT - 75}{250 - 75} * 100 \text{ if } 75\ \mu g\ m^{-3} < CWT < 250\ \mu g\ m^{-3} \\ 100 \text{ if } CWT \geq 250\ \mu g\ m^{-3} \end{cases}
$$

(1)

Based on the above calculation, all emissions will be shut off or grid cells with $CWT \geq 250 \mu g\, m^{-3}$, while those will remain uncontrolled for grid cells with $CWT \leq 75 \mu g\, m^{-3}$. For grid cells with $75 \mu g\, m^{-3} < CWT < 250 \mu g\, m^{-3}$, the ECFs are calculated as (CWT-75)/(250–75) with (250–75) as the scaling factor. The concentration of $75 \mu g\, m^{-3}$ is China's national daily secondary ambient air quality standard for $PM_{2.5}$, which we take as the control objective. To assess the effectiveness of the PAPCA strategy, emission controls were applied to the entire region 48-h prior to the time of the forecasted onset of the severe haze episode (i.e., hourly $PM_{2.5} \geq 150 \mu g\, m^{-3}$) (Fig. 3). Temporal variations and reductions of $PM_{2.5}$ concentrations during the haze periods for the four different emission control scenarios (ECS) on the basis of the CWT value intervals (i.e., ECS1: $75 \mu g\, m^{-3} \leq CWT < 115 \mu g\, m^{-3}$; ECS2: $115 \mu g\, m^{-3} \leq CWT < 150 \mu g\, m^{-3}$; ECS3: $150 \mu g\, m^{-3} \leq CWT < 250 \mu g\, m^{-3}$; ECS4: $CWT \geq 250 \mu g\, m^{-3}$) are shown in Figs 3 and S1c.

Model simulations in Figs 3 and S19 show that peak $PM_{2.5}$ concentrations are predicted to be effectively decreased by more than 60% to a level below ~$100 \mu g\, m^{-3}$ for each severe urban haze outbreak when the PAPCA strategies are applied to the targeted areas with $150 \mu g\, m^{-3} \leq CWT < 250 \mu g\, m^{-3}$ (i.e., ECS3 case) or $CWT \geq 250 \mu g\, m^{-3}$ (i.e., ECS 4 case). By contrast, peak $PM_{2.5}$ concentrations are predicted to be decreased by only $<25\%$ if the emission control strategies are applied to the targeted areas with $CWT \leq 150 \mu g\, m^{-3}$ (i.e., cases ECS1 and ECS2) (Figs 3 and S19). For example, the simulated mean $PM_{2.5}$ concentration for the period from 22:00 on October 26 to 16:00 on October 28 in Beijing decreased from $203.0 \mu g\, m^{-3}$ to 198.8, 192.9, 79.8, and $74.0 \mu g\, m^{-3}$ for the emission control scenarios ECS1, ECS2, ECS3 and ECS 4, respectively (Fig. S1c). For the severe haze period from 7:00 on October 31 to 3:00 on November 2 in Beijing, the mean $PM_{2.5}$ concentration decreased from $224.4 \mu g\, m^{-3}$ to 217.0, 205.7, 77.8, and $56.9 \mu g\, m^{-3}$ for the cases ECS1, ECS2, ECS3 and ECS 4, respectively (Fig. S1c). Similar results for the effectiveness of the PAPCA for the severe haze episodes in Shanghai (Fig. 3b), Hangzhou (Fig. 3c), Xian (Fig. 3d) and 2017 Beijing case (Fig. 3a) are obtained (see SI). Fig. S19 summarizes the $PM_{2.5}$ reduction as a function of the emission control scenarios in terms of the CWT value intervals.

To test the practicality of the PAPCA, three emission control scenarios (i.e., cases 1, 3, and 5) were designed by controlling only transportation and industrial emissions instead of all emission sources based on the ECF values as summarized in Table 1. The Beijing government suspended 50% vehicle traffic and production operations at about 2,100 companies in Beijing when the smog red alert was issued on December 7, 2015[18]. Cases 1, 3 and 5 in Table 1 are designed for the PAPCA to control emissions over only targeted areas with $CWT \geq 150 \mu g\, m^{-3}$ (see Fig. 2e) for 50% vehicle emission controls, but different industrial emission control percentages (i.e., 75%, 50%
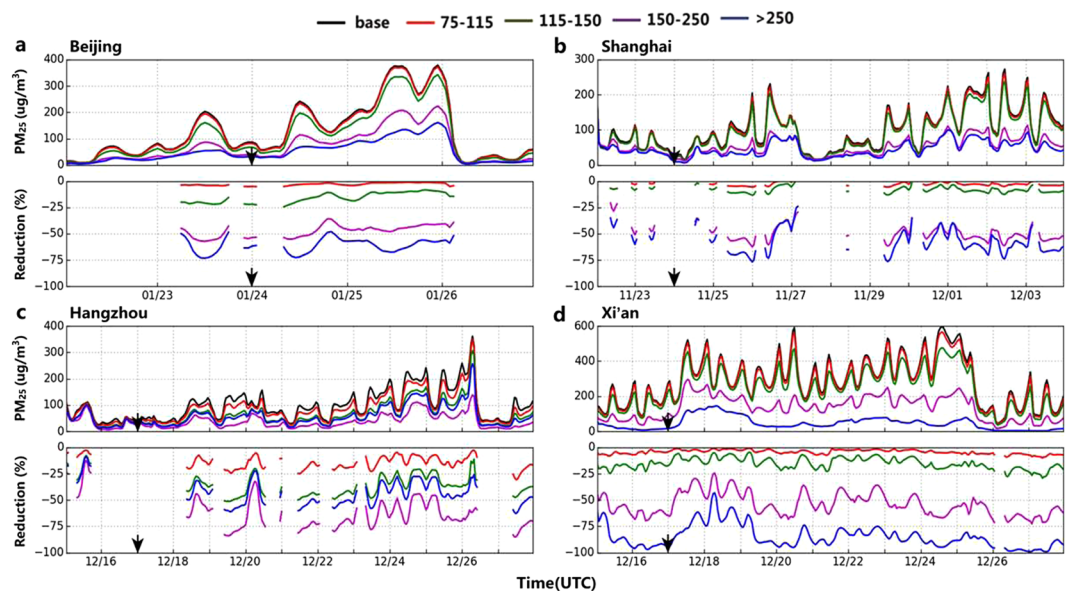
Figure 3. Test of effectiveness of the PAPCA strategy for the four different emission control scenarios. (**a**) Temporal variations of hourly mean $PM_{2.5}$ concentrations and their reduction relative to the base case for the four different emission control scenarios on the basis of the four different CWT value intervals in Beijing for the period from Jan 22 to 26, 2017. The proportional reduction is given only when the hourly mean $PM_{2.5}$ concentrations exceed $75\,\mu g\,m^{-3}$. (**b**) The same as (**a**) but for the period from Nov 24 to Dec 4, 2013, in Shanghai. (**c**) The same as (**a**) but for the period from December 15 to Dec 28, 2013, in Hangzhou. (**d**) The same as (**a**) but for the period from December 15 to Dec 28, 2013, in Xi'an. The arrow symbols represent the day with the hourly $PM_{2.5} \geq 150\,\mu g\,m^{-3}$ forecasted. The arrow signs show the heavy haze day with hourly mean $PM_{2.5}$ concentration $>150\,\mu g\,m^{-3}$ at least in one hour and 48 hours earlier than this heavy haze day is the time to start emission control schemes.

Cases	Transportation	Industry	Controlling Areas
Case1	−50%	−75%	Target Areas
Case2	−50%	−75%	Surrounding Areas
Case3	−50%	−50%	Target Areas
Case4	−50%	−50%	Surrounding Areas
Case5	−50%	−25%	Target Areas
Case6	−50%	−25%	Surrounding Areas
Case7	−100%	−100%	For the city only

Table 1. Emission control scenarios for testing the PAPCA*. *Surrounding areas: (1) For Beijing, its surrounding area includes Beijing-Tianjing-Hebei; (2) For Shanghai and Hangzhou, it is Yangtze River Delta (Shanghai-Jiangsu-Zhejiang-Anhui); (3) For Xian, its surrounding area is Shanxi province (see Fig. 1). Target areas refer to the areas identified by the CWT values in the PAPCA strategy.

and 25%, respectively), depending on the air quality objectives. CWT $\geq 150\,\mu g\,m^{-3}$ is chosen because the results in Fig. 3 show that the peak $PM_{2.5}$ concentrations can be effectively decreased by $>60\%$ when the approach is applied to the targeted areas with CWT $\geq 150\,\mu g\,m^{-3}$. Case 7 in Table 1 tests the extent to which air quality can be significantly improved when all emissions in the studied city are suspended.

Fig. S20a, S20b show the temporal variations and reductions of $PM_{2.5}$ concentrations in the five cities for the different cases, and the results are summarized in Figs 4, S19a and S19b. For case 1 with emission controls from 50% vehicles and 75% industries, the mean $PM_{2.5}$ concentration for the severe haze periods in Beijing (from 22:00 on October 26 to 16:00 on October 28, 2103), Beijing (from 9:00 on January 24 to 3:00 on January 26, 2017), Shanghai (from 10:00 on December 1 to 14:00 on December 3), and Xian (from 9:00 on December 16 to 14:00 on December 25) decreased from $203.0\,\mu g\,m^{-3}$ to $95.7\,\mu g\,m^{-3}$, $245.9\,\mu g\,m^{-3}$ to $166.1\,\mu g\,m^{-3}$, $172.1\,\mu g\,m^{-3}$ to $71.0\,\mu g\,m^{-3}$, and $347.9\,\mu g\,m^{-3}$ to $174.4\,\mu g\,m^{-3}$, respectively. Since emissions are assumed to be controlled only for two sectors (transportation and industries), the results in Figs 4, S1d, S20a, S20b, S19a and S19b demonstrate the essential nature of the PAPCA. In case 7, for which complete emission control in each city is implemented, the mean $PM_{2.5}$ concentration for the haze periods in Beijing (2013 case), Beijing (2017 case), Shanghai, and Xian are predicted to be decreased from $203.0\,\mu g\,m^{-3}$ to $177.9\,\mu g$ mrespectively. Since emissions are assumed, $245.9\,\mu g\,m^{-3}$ to $237.3\,\mu g\,m^{-3}$, $172.1\,\mu g\,m^{-3}$ to $153.7\,\mu g\,m^{-3}$, and $347.9\,\mu g\,m^{-3}$ to $268.5\,\mu g\,m^{-3}$, respectively. This comparison highlights the fact that, in certain cases, local emissions from the city are
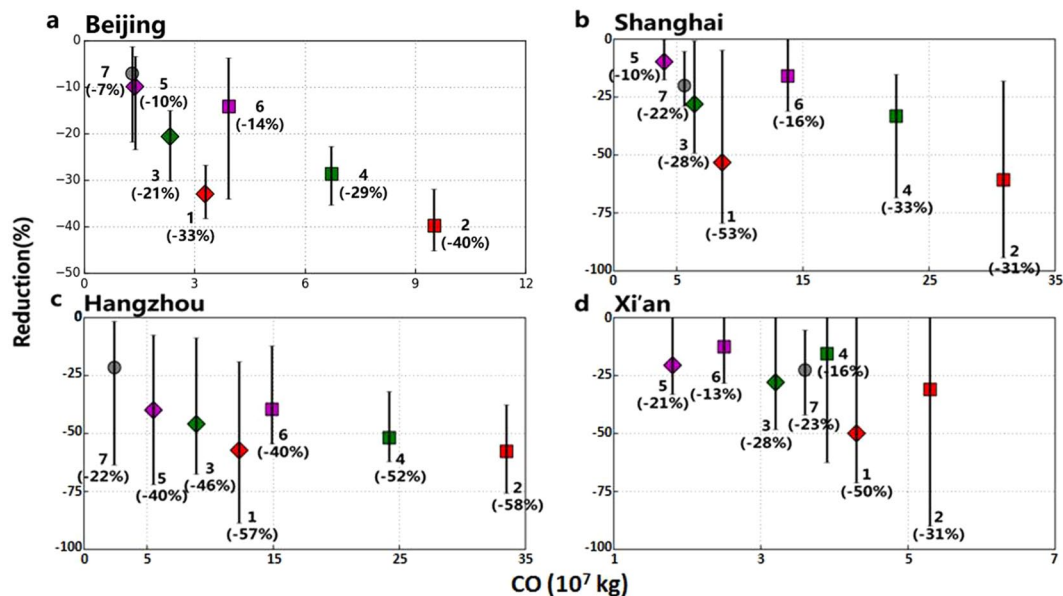
Figure 4. $PM_{2.5}$ reduction percentages as a function of the emission control amounts for the test of economic efficiency of the PAPCA. (**a**) The mean $PM_{2.5}$ reduction as a function of the CO emission control amounts for the 6 different cases in Beijing. Numbers 1–7 refer to the corresponding cases in Fig. S15 and Table 2. The same colors represent the pair comparisons (e.g., cases 1 and 2 are the pair). The ranges of the reduction percentages are calculated on the basis of the hourly results for the periods. Here we use CO emission control amounts as the x-axis to represent the general emission controls because CO is a long-lived tracer of human activity associated with sources, such as combustion, industry, mobile, and hydrocarbon oxidation. (**b**) The same as (**a**) but for Shanghai. (**c**) The same as (a) but for Hangzhou. (**d**) The same as (a) but for Xian.

not primarily responsible for the severe haze episode, as even when emissions in each city are totally curtailed, mean $PM_{2.5}$ concentrations in Beijing (2013 case), Beijing (2017 case), Shanghai, Hangzhou and Xian are predicted to be reduced only by 11.1%, 7%, 22.0%, 21.5% and 22.6%, respectively (Figs 4 and S1d and Tables 2 and S7).

Cases 2, 4 and 6 in Table 1 are designed to replicate emission control for two sectors (transportation and industries) in each city and its surroundings, as this represents the actual strategy used by the government during the smog red alert[18]. Comparisons between the results of these cases (Cases 2, 4, and 6) and their corresponding cases (Cases 1, 3, and 5) in Figs 4, S1d, S19a, 19b, 20a and 20b and Tables 2 and S7 reveal that relative to those of the Cases 2, 4, and 6, the PAPCA strategy (Cases 1, 3, and 5) can significantly reduce the comparable $PM_{2.5}$ concentrations but with ~30% to ~70% less emission controls. For example, predicted emission reductions needed by the PAPCA for CO, SO_2, NO_x, VOC, primary $PM_{2.5}$ ($pPM_{2.5}$), primary coarse PM (PMcoarse), BC and OC in case 1 in Beijing (2013 case) are 23.7, 24.6, 30.2, 27.4, 12.4, 6.3, 1.7, 1.5 10^4 tons, respectively, about 22% to 26% less than the corresponding values for case 2 (see Table S7). Similar results can be obtained for the Beijing case in 2017 (see Table 2). Note that the significant differences in total emission control amounts between the 2013 and 2017 cases in Beijing as shown in Tables 2 and S7 is due to the fact that the heavy haze episode in 2013 lasted much longer and was affected by broader source regions relative to those in 2017 Beijing case. The emission control times for the Beijing case in 2013 and 2017 are from 00:00 on January 22 to 24:00 on January 26, 2017 (total 120 hours) and from 00:00 on October 24 to 24:00 on November 3, 2013 (total 264 hours). The results for the Beijing case in 2013 retrospective simulations and in 2017 forecast simulations indicate that the PAPCA works well for the same city but under different pollution episodes with the meteorological conditions that are totally different. For Shanghai, predicted emission reductions needed by the PAPCA for CO, SO_2, NO_x, VOC, primary $PM_{2.5}$ ($pPM_{2.5}$), primary coarse PM (PMcoarse), BC and OC in cases 1, 3 and 5 are about 64% to 75% less than the corresponding values for the cases 2, 4 and 6, while for Hangzhou city, they are about 55% to 67% less (Table 2). In Xian, the results are summarized for the comparisons in Shaanxi province only because the severe haze episode in Xian was caused by the air masses from the surrounding industrialized cities in all directions (see Figs 2d and S5). Table 2 shows that the PAPCA emission reductions needed for CO, SO_2, NO_x, VOC, primary $PM_{2.5}$ ($pPM_{2.5}$), primary coarse PM (PMcoarse), BC and OC in cases 1, 3, and 5 are about 5% to 29% less than the corresponding values for cases 2, 4 and 6 in Xian city.

Methods

Precision air pollution control approach (PAPCA). The PAPCA involves three steps (Fig. S21). The first step is to identify an impending period with high $PM_{2.5}$ concentrations and time to start emission control schemes. Here, we have considered hourly mean $PM_{2.5}$ concentration $\geq 150\,\mu g\,m^{-3}$ to define a severe urban haze event for the city. For example, the arrow signs in Fig. 3 show the heavy haze day with hourly mean $PM_{2.5}$ concentration $> 150\,\mu g\,m^{-3}$ at least in one hour and 48 hours earlier than this heavy haze day is the time to initiate

Case	PM$_{2.5}$ reduction (%)	Emission reduction (10^7 kg)								
		CO	SO$_2$	NH$_3$	NO$_x$	VOC	PM$_{2.5}$	PMcoarse	BC	OC
Beijing (2017)										
1	−33.0	3.3	0.3	0.004	0.4	3.8	0.2	0.08	0.6	0.5
2	−39.7	9.5	1.1	0.01	1.1	10.2	0.5	0.2	1.8	1.7
3	−20.7	2.3	0.2	0.003	0.3	2.7	0.1	0.05	0.5	0.4
4	−28.7	6.7	0.7	0.01	0.9	7.2	0.3	0.2	1.4	1.2
5	−9.9	1.4	0.1	0.002	0.2	1.5	0.05	0.01	0.3	0.2
6	−14.2	3.9	0.4	0.006	0.6	4.2	0.2	0.08	0.9	0.7
7	−7.1	1.3	0.2	0.002	0.3	3.5	0.07	0.04	0.3	0.2
Shanghai										
1	−53.2	8.6	13.2	0.4	16.5	35.0	7.8	4.1	0.9	0.8
2	−60.7	30.9	45.9	1.0	65.2	99.4	21.5	12.6	2.8	2.3
3	−28.0	6.4	8.7	0.2	12.9	23.9	5.3	2.7	0.7	0.6
4	−33.2	22.4	30.8	0.7	50.3	68.2	14.8	8.4	2.1	1.6
5	−9.8	4.0	4.5	0.1	9.3	12.9	2.9	1.4	0.5	0.3
6	−15.9	13.8	15.8	0.4	35.3	37.0	8.1	4.2	1.4	1.0
7	−22.0	5.6	1.3	0.1	1.6	2.0	0.3	0.1	0.03	0.03
Hangzhou										
1	−38.5	12.3	22.2	0.5	26.1	35.0	8.8	5.0	1.1	0.9
2	−43.3	33.5	49.7	1.1	70.7	107.6	23.3	13.6	3.0	2.4
3	−23.7	8.9	14.9	0.3	20.0	24.1	6.1	3.3	0.9	0.7
4	−33.4	24.2	33.4	0.7	54.5	73.9	16.0	9.1	2.3	1.7
5	−14.5	5.5	7.6	0.2	14.0	13.2	3.3	1.7	0.6	0.4
6	−15.2	14.9	17.1	0.4	38.3	40.1	8.7	4.6	1.5	1.0
7	−21.5	2.4	0.3	0.1	0.7	1.1	0.2	0.1	0.02	0.02
Xi'an										
1	−49.9	4.3	14.6	0.7	9.6	11.8	4.3	2.8	0.7	0.9
2	−31.0	5.3	19.6	1.1	10.7	13.5	5.3	3.1	1.0	1.0
3	−27.9	3.2	11.8	0.6	7.5	8.5	3.2	1.8	0.5	0.5
4	−15.6	3.9	13.2	1.0	8.2	9.3	3.6	2.1	0.5	0.6
5	−20.6	1.8	5.0	0.5	5.7	4.6	1.8	0.7	0.4	0.4
6	−12.6	2.5	6.8	0.5	5.8	5.3	1.8	1.1	0.5	0.4
7	−22.6	3.6	0.7	0.4	0.7	0.4	0.4	0.2	0.1	0.1

Table 2. PM$_{2.5}$ reduction and emission control amounts for each species for each case.

emission control schemes. The second step is to calculate the concentration weighted trajectory (CWT) values for PM$_{2.5}$ using the hybrid receptor model with 48-h back trajectories and PM$_{2.5}$ concentrations (SI Appendix) to pinpoint source areas leading to high PM$_{2.5}$ levels. Note that the PM$_{2.5}$ trigger concentrations can arise from either observations or model forecasts at the receptor sites when the CWT values are calculated. The third step is to employ a comprehensive atmospheric chemical transport model (CTM) (here the two-way coupled WRF-CMAQ) to optimize emission controls using the CWT values as a weighting function as shown in equation (1). This last step involves a series of CTM simulations to determine the optimal emission control scenarios. In summary, in the PAPCA used in forecast mode, the period of the high PM$_{2.5}$ concentrations is identified by the 3-D CTM forecast, and the CWT values for PM$_{2.5}$ are calculated using the hybrid trajectory-receptor model with 48-h back trajectories on the basis of forecast meteorological fields and forecast PM$_{2.5}$ concentrations. Note that the meteorological initial and lateral boundary conditions were derived from the Global Forecast System (GFS) model data when the PAPCA is used in forecast mode and the meteorological initial, and lateral boundary conditions were derived from the National Center for Environmental Prediction (NCEP) final analysis dataset in the retrospective simulations.

Observations and hybrid receptor model. Hourly PM$_{2.5}$, O$_3$, SO$_2$, NO$_2$ and CO concentrations at four cities (at 12, 10, 8 and 9 monitoring stations in Beijing, Shanghai, Hangzhou and Xian, respectively) were obtained from the national air quality monitoring network operated and maintained by the Ministry of Environmental Protection (MEP) in China (http://datacenter.mep.gov.cn/). The observations of PM$_{2.5}$ Chemical Composition for each case study were also obtained on the basis of the available field study. More details are available in the SI Appendix.

The 48-h back trajectories starting at the arrival level of 100 m from the monitoring sites were calculated with the NOAA HYSPLIT model (http://ready.arl.noaa.gov/HYSPLIT.php) for each period. Back trajectories were calculated eight times per day at starting times of 00:00, 03:00, 6:00, 09:00, 12:00, 15:00, 18:00 and 21:00 UTC. Based on the results of the HYSPLIT model, the CWT method can be used to pinpoint regional sources with significant

potential contributions of high CWT values to receptor site concentrations. The CWT value (CWT_{ij}) for grid cell (i,j) is calculated as the average weighted concentration by the following equation[36–40]:

$$CWT_{ij} = \frac{1}{\sum_{l=1}^{M} T_{ijl}} \sum_{l=1}^{M} C_l T_{ijl},$$

where C_l and T_{ijl} are the concentration at the receptor site on the arrival of trajectory l and the time spent in the grid cell (i, j) for the trajectory, respectively, and l and M are the index and total number of the trajectories, respectively. Note that since the targeted areas with the highest potential contributions to the haze episode identified by the CWT values vary for different episodes, the optimal emission control schemes are determined for each particular situation.

Two-way coupled WRF-CMAQ modeling system. We have used the two-way coupled WRF-CMAQ[41,42] to simulate urban PM$_{2.5}$ events. A series of simulations for different emission control scenarios were conducted to assess the optimal emission control scheme for the targeted areas. The WRF-CMAQ system was developed by linking Weather Research and Forecast (WRF, version 3.4) and Community Multiscale Air Quality (CMAQ, version 5.0)[41–44]. The model configurations are the same as those in Yu et al.[42]. The modeling domain covers most of China and parts of East Asia with 12 km × 12 km grid resolution and with 27 vertical layers for both WRF and CMAQ (see Fig. S6). The physics package of the WRF3.4 (ARW) includes the Kain–Fritsch (KF2) cumulus cloud parameterization, the Asymmetric Convective Model (ACM2) for a planetary boundary layer (PBL) scheme, RRTMG shortwave and longwave radiation schemes, two-moment cloud microphysics, and the Pleim–Xiu (PX) land-surface scheme. In the retrospective simulations, the meteorological initial, and lateral boundary conditions for the outermost domain were derived from the National Center for Environmental Prediction (NCEP) final analysis dataset with a spatial resolution of 1° × 1° and a temporal resolution of 6 h. In the forecast simulations, the meteorological initial and lateral boundary conditions were derived from the Global Forecast System (GFS) model data. The carbon bond chemical mechanism (CB05)[45] is used to represent gas-phase photochemical reaction pathways, and the AERO6 aerosol module of CMAQ version 5.0 is used to represent aerosol microphysics. The default chemical boundary conditions (BCONs) in the CMAQ model were used in the simulations. For both retrospective and forecast simulations, anthropogenic emissions of SO$_2$, NO$_x$, CO, NMVOC, NH$_3$, PM$_{10}$ and PM$_{2.5}$ over China were based on the Multi-resolution Emission Inventory for China (MEIC)[46] for 2012 (www.meicmodel.org), while those over the rest of domain were estimated on the basis of Emissions Database for Global Atmospheric Research (EDGAR): HTAP V2 (0.1° × 0.1°). Multi-resolution Emission Inventory for China (MEIC) is a dynamic technology-based inventory for more than 700 anthropogenic emitting sources developed for China covering the years from 1990 to 2013 by Tsinghua University following the work of INTEX-B[46]. With the detailed source classification by representing emission characteristics of different sectors, fuels, products, emission control and combustion/process technologies, the MEIC model can derive emissions which are aggregated to five sectors: power plants, industries, residential, transportation, and agriculture[43]. For example, transportation emissions at high spatial resolution were derived on the basis of vehicle population and emission factors at county level, while the emissions at high-resolution model grids can be derived on the basis of the county-level emissions and information about a digital road map and weighting factors of traveling kilometers and road types[46]. The lumped speciated NMVOC emissions were derived for each source sector by splitting the total NMVOC emissions according to the speciation assignment approaches for different chemical mechanisms such as CB05 in the MEIC43. Temporal variations and gridded emissions were created for each sector using different temporal profiles and spatial aggregations[46]. The detailed description of the MEIC can be found in Li et al.[46]. Note that since the heating in southern and northern China is different, the contribution of residential emissions in terms of heating to the haze formation will be significantly different.

Model performance evaluations. Evaluation of the WRF-CMAQ model performance of PM$_{2.5}$, PM$_{10}$, NO$_2$, SO$_2$, CO, and PM$_{2.5}$ chemical composition for the studied four severe urban haze episodes for each city are summarized in Tables S2–S6. Figs S7–S18 show time-series comparisons of mean observed and predicted concentrations of different species for each city and its related surrounding cities for the five severe urban haze cases. As can be seen, the model captures the spatial pattern of most of observations reasonably well for this severe haze episode. For the Beijing case in 2013, the NMB values for PM$_{2.5}$ range from 0.2% at Handan to −19.5% at Qinhuangdao at all related cities except Tangshan where the NMB value for PM$_{2.5}$ is 45.8% (see Table S2). For the Shanghai case, the NMB values for PM$_{2.5}$ range from 5.6% at Changzhou to −26.2% at Ningbo (see Table S3). For the Hangzhou case, the NMB values for PM$_{2.5}$ are within ±25% except for Huaian, Huzhou, and Lianyungang where the NMB values for PM$_{2.5}$ are −35.9%, −37.1% and −45.8%, respectively (see Table S4). For the Xian case, The NMB values for PM$_{2.5}$ range from −11.1% at Xian to −37.1% at Tongchuan (see Table S5). Model performances for PM$_{2.5}$ chemical composition on the basis of available measurements for the Beijing, Shanghai, Hangzhou and Xian cases in the retrospective simulations are summarized in Tables S6a, S6b, S6c and S6d, respectively. The temporal variations of comparisons of predictions and observations for each PM$_{2.5}$ component are shown in Figs S15–S18. The model simulations generally underestimate both SO$_4^{2-}$ and NH$_4^+$ at urban sites (Beijing, Zhengzhou, and Xian sites) but overestimate both SO$_4^{2-}$ and NH$_4^+$ at the rural sites (Linan, Taiyangshang and Gaolanshan) for all four heavy haze episodes, while the model simulations overestimate EC at all sites and cases except the Beijing case at Zhengzhou site where the model simulations slightly underestimate observed EC by −3.5% (see Table S6a). The model simulations underestimate OC at all sites and cases except the Shanghai case at Taiyangshan site where the model simulations slightly overestimate observed OC by 13.3% (see Table S6b), while the model simulations underestimate NO$_3^-$ at all sites and cases except the Beijing case at the Beijing site and Xian case at Xian site where the model simulations overestimate NO$_3^-$ slightly. Uncertainties in

emission inventories, the physical-chemical mechanisms of haze formation, and prognostic model simulation of meteorological fields are the sources of biases in the simulations of $PM_{2.5}$ chemical composition. More details about model performance are available in the SI Appendix.

Uncertainties associated with the PAPCA strategy.   There are recognizable uncertainties associated with the PAPCA strategy. First, simulations of the severe haze episodes (i.e., high $PM_{2.5}$ concentrations) by the 3-D air quality models (WRF-CMAQ here) involve inevitable uncertainties in emission inventories[32], the physical-chemical mechanisms of haze formation, and prognostic model forecasts of meteorological fields. Emissions-modeling uncertainties involve inventory emissions for area, line and point sources, temporal profiles, chemical speciation profiles, spatial surrogates and vertical distribution[47]. Although the anthropogenic emission inventory for China used in this study was derived from the extensively tested state-of-the-art MEIC model (includes five anthropogenic source sectors: power, industry, transportation, residential, and agriculture)[48], uncertainties remain at high spatial and temporal resolutions. Severe winter haze events over the North China Plain have not been captured successfully by a number of air quality models, indicating that the physical-chemical mechanisms of haze formation may not yet be completely understood[49]. Despite the overall strong performance of the two-way coupled WRF-CMAQ model for these five severe urban haze episodes, further in-depth evaluation of model predictions is warranted.

Uncertainties in the hybrid receptor model can affect the accuracy in determination of source origins of severe haze pollution and in optimization of the emission control schemes for the targeted areas. Despite the fact that the HYSPLIT model is a well-tested system for computing air parcel back-trajectories[50], complex wind fields can lead to uncertain prediction of trajectories because of neglect of wind shear in the trajectory calculations[51]. Nevertheless, it is established that the trajectory model may be accurately employed for various regimes of stability, wind shear and source configuration[51]. Since the high $PM_{2.5}$ concentrations are the result of primary emissions and secondary aerosol production, the CWT values, which are calculated on the basis of $PM_{2.5}$ concentrations at the receptor site and the arrival of back-trajectories (see Methods), contain the information about the sources of primary emissions and chemical transformation. That implementation of the PAPCA is predicted to effectively reduce the $PM_{2.5}$ peak concentrations for the five severe urban haze episodes using the CWT values as weighted function suggests that the CWT values successfully pinpoint the source origins of the severe urban haze pollution.

References

1. Normile, D. China rethinks cities. *Science* **352**, 917–918 (2016).
2. Kelly, F. J. & Zhu, T. Transport solutions for cleaner air. *Science* **352**, 934–936 (2016).
3. Kulmala, M. China's choking cocktail. *Nature* **526**, 497–499 (2015).
4. Liu, J. *et al*. Air pollutant emissions from Chinese households: A major and underappreciated ambient pollution source. *Proc. Natl. Acad. Sci. USA* **113**, 7756–7761 (2016).
5. The General Office of the State Council of China: Circular on Forwarding the Guidance of Promoting Joint Prevention and Control of Air Pollution and Improving the Regional Air Quality, Issued by MEP and other Government Agencies, http://www.gov.cn/xxgk/pub/govpublic/mrlm/201005/t20100513_56516.html [accessed May 3, 2018] (2010).
6. Guo, S. *et al*. Elucidating severe urban haze formation in China. *Proc. Natl. Acad. Sci. USA* **111**, 17373–17378 (2014).
7. Huang, R. *et al*. High secondary aerosol contribution to particulate pollution during haze events in China. *Nature*. **514**, 218–222 (2014).
8. He, H. *et al*. Formation Mechanism and Control Strategies of Haze in China. *Bull. of Chin. Academy of Sci.* **28**, 344–352 (2013).
9. Zhang, X. *et al*. Factors contributing to haze and fog in China (in Chinese). *Chin. Sci. Bull.* **58**, 1178–1187 (2013).
10. Yu, S. *et al*. Origin of air pollution during a weekly heavy haze episode in Hangzhou, China. *Environ. Chem. Lett.* **12**, 543–550 (2014).
11. Chan, C. & Yao, X. Review: air pollution in megacities in China. *Atmos. Environ.* **42**, 1–42 (2008).
12. Shao, M., Tang, X., Zhang, Y. & Li, W. City clusters in China: air and surface water pollution. *Front. Ecol. Environ.* **4**, 353–361 (2006).
13. Sun, Y. *et al*. Long-term real-time measurements of aerosol particle composition in Beijing, China: seasonal variations, meteorological effects, and source analysis. *Atmos. Chem. Phys.* **15**, 10149–10165 (2015).
14. Yu, S. *et al*. Anthropogenic aerosols are a potential cause for migration of the summer monsoon rain belt in China. *Proc. Natl. Acad. Sci. USA* **113**, E2209–E2210 (2016).
15. Li, P. *et al*. Reinstate regional transport of $PM_{2.5}$ as a major cause of severe haze in Beijing. *Proc. Natl. Acad. Sci. USA* **112**, E2739–E2740 (2015).
16. Liao, H., Chang, W. & Yang, Y. Climatic effects of air pollutants over China: A review. *Adv. Atmos. Sci.* **32**, 115–139 (2015).
17. China's State Council, Atmospheric Pollution Prevention and Control Action Plan, http://english.mep.gov.cn/News_service/infocus/201309/t20130924_260707.htm [accessed May 3, 2018] (2013).
18. Sina News, Beijing starts emergency response measures as smog continues, http://english.sina.com/china/p/2013/0113/548263.html [accessed May 3, 2018] (2013).
19. Xinhua News, Solving heavy haze: What can we do for the lock fog and haze in China? http://www.gov.cn/jrzg/2014-02/18/content_2612582.htm [accessed May 3, 2018] (2014).
20. The Ministry of Environmental Protection of China, Air quality status in key regions and 74 cities in China in January-February and February, 2017 http://www.mep.gov.cn/gkml/hbb/qt/201703/t20170324_408728.htm [accessed May 3, 2018] (2017).
21. Hao, N. & Liu, C., 80% of Chinese cities flunk air quality standard. http://english.sepa.gov.cn/News_service/media_news/201701/t20170118_394942.shtml [accessed May 3, 2018] (2017).
22. The Ministry of Environmental Protection (MEP) of China, MEP releases the air quality status of key regions and 74 cities in January 2017. http://english.mep.gov.cn/News_service/news_release/201702/t20170223_397379.shtml [accessed May 3, 2018] (2017).
23. Guo, S. *et al*. Quantitative evaluation of emission controls on primary and secondary organic aerosol sources during Beijing 2008 Olympics. *Atmos. Chem. Phys.* **13**, 8303–8314 (2013).
24. Huang, X. *et al*. Highly time-resolved chemical characterization of atmospheric fine particles during 2010 Shanghai World Expo. *Atmos. Chem. Phys.* **12**, 4897–4907 (2012).
25. Chen, C. *et al*. Characteristics and sources of submicron aerosols above the urban canopy (260m) in Beijing, China, during the 2014 APEC summit. *Atmos. Chem. Phys.* **15**, 12879–12895 (2015).
26. CCN, Blue sky vanishes immediately after Beijing's massive parade, http://edition.cnn.com/2015/09/04/asia/china-beijing-blue-sky-disappears-after-military-parade/ [accessed May 3 2018] (2015).
27. Li, P. *et al*. High reduction of ozone and particulate matter during the 2016 G-20 summit in Hangzhou by forced emission controls of industry and traffic. *Environ. Chem. Lett.* **15**(4), 709–715 (2017).

10

28. Wang, P. & Dai, X. G. "APEC Blue" association with emission control and meteorological conditions detected by multi-scale statistics. *Atmos. Res.* **178–179**, 497–505 (2016).
29. Ugrin, E., Red alert for smog pollution issued in Beijing, China. https://watchers.news/2015/12/08/red-alert-for-smog-pollution-issued-in-beijing-china/ [accessed May 3 2018] (2015).
30. China daily, Seven urgent questions about Beijing's first red smog alert. http://www.chinadaily.com.cn/china/2015-12/08/content_22660890.htm [accessed May 3 2018] (2015).
31. China daily, Red alert helps to reduce pollutants, say experts. http://usa.chinadaily.com.cn/china/2015-12/10/content_22685490.htm [accessed May 3 2018] (2015).
32. Russel, A. & Dennis, D. NARSTO critical review of photochemical models and modeling. *Atmos. Environ.* **34**, 2283–2324 (2000).
33. Belis, C. A., Karagulian, F., Larsen, B. R. & Hopke, P. K. Critical review and meta-analysis of ambient particulate matter source apportionment using receptor models in Europe. *Atmos. Environ.* **69**, 94–108 (2013).
34. Schauer, J. J. *et al.* Source apportionment of airborne particulate matter using organic compounds as tracers. *Atmos. Environ.* **30**, 3837–3855 (1996).
35. Hopke, P. K., The application of receptor modeling to air quality data. *Pollution Atmospherique*, 91-109 (2010).
36. Yan, R. *et al.* A heavy haze episode in Beijing in February of 2014: Characteristics, origins and implications. *Atmos. Pollut. Res.* **6**, 867–876 (2015).
37. Zhang, Q. *et al.* A heavy haze episode in Shanghai in December of 2013: Characteristics, origins, and implications. *Aerosol and Air Quality Research* **15**, 1881–1893 (2015).
38. Hsu, Y. K., Holsen, T. M. & Hopke, P. K. Comparison of hybrid receptor models to locate PCB sources in Chicago. *Atmos. Environ.* **37**, 545–562 (2003).
39. Wang, Y., Zhang, X. & Draxler, R. R. TrajStat: GIS-based software that uses various trajectory statistical analysis methods to identify potential sources from long-term air pollution measurement data. *Environ Model Software* **24**, 938–939 (2009).
40. Wang, S. *et al.* Characteristics and origins of air pollutants in Wuhan, China, based on observations and hybrid receptor models. *J. Air & Waste Manage Assoc* **67**(7), 739–753 (2017).
41. Wong, D. C. *et al.* WRF-CMAQ two-way coupled system with aerosol feedback: software development and preliminary results. *Geosci. Model Dev.* **5**, 299–312 (2012).
42. Yu, S. *et al.* Aerosol indirect effect on the grid-scale clouds in the two-way coupled WRF-CMAQ: model description, development, evaluation and regional analysis. *Atmos. Chem. Phys.* **14**, 11247–11285 (2014).
43. Skamarock, W. C. *et al. A description of the advanced research WRF version 3.* NCAR Technical Note NCAR/TN-475+STR, *NCAR* (2008).
44. Eder, B. & Yu, S. An evaluation of model performance of EPA models-3/CMAQ. *Atmos. Environ.* **40**, 4811–4824 (2006).
45. Yarwood, G., Rao, S., Yocke, M. & Whitten, G. Z. Updates to the Carbon Bond Chemical Mechanism: CB05.Final report to the US EPA, Rep. RT-04-00675, 246 pp., Yocke and Co., Novato, California, http://www.camx.com/publ/pdfs/CB05_Final_Report_120805.pdf [accessed June 2017] (2005).
46. Li, M. *et al.* MIX: a mosaic Asian anthropogenic emission inventory under the international collaboration framework of the MICS-Asia and HTAP. *Atmos. Chem. Phys.* **17**, 935–963 (2017).
47. Houyoux, M. R. *et al.* Emission inventory development and processing for the Seasonal Model for Regional Air Quality (SMRAQ) project. *J. Geophys. Res.* **105**, 9079–9090 (2000).
48. Liu, F. *et al.* High-resolution inventory of technologies, activities, and emissions of coal-fired power plants in China from 1990 to 2010. *Atmos. Chem. Phys.* **15**, 13299–13317 (2015).
49. Cheng, Y. *et al.* Reactive nitrogen chemistry in aerosol water as a source of sulfate during haze events in China. *Sci. Adv.* **2**, e1601530 (2016).
50. Draxler, R. R. & Hess, G. D. An overview of the HYSPLIT_4 modeling system for trajectories, dispersion and deposition. *Aust. Meteor. Mag.* **47**, 295–308 (1998).
51. Liu, M. & Seinfeld, J. On the validity of grid and trajectory models of urban air pollution. *Atmos. Environ.* **9**, 555–574 (1975).

Acknowledgements

Author Contributions

S.Y., K.A. and J.H.S. initiated the project and designed the experiments; S.Y., P.L., L.W., Y.W. and J.H.S. wrote the main manuscript. S.Y., P.L., L.W., Y.W., S.W., K.L., T.Z., Y.Z., M.H., L.Z., X.Z., J.C., K.A., D.W., J.P., R.M., D.R. and J.H.S. contributed to the interpretation and to manuscript preparation.

Additional Information

Supplementary information accompanies this paper at https://doi.org/10.1038/s41598-018-26344-1.

Competing Interests: The authors declare no competing interests.

Publisher's note: Springer Nature remains neutral with regard to jurisdictional claims in published maps and institutional affiliations.